Computational Materials Science 145 (2018) 48–59

Contents lists available at ScienceDirect

Computational Materials Science

journal homepage: www.elsevier.com/locate/commatsci

Mathematical modeling of reverse atom transfer radical polymerization in miniemulsion

A. Zurman [a], C. Sarmoria [a,b], A. Brandolin [a,b], M. Asteasuain [a,b,*]

[a] Planta Piloto de Ingeniería Química (PLAPIQUI), CONICET-UNS, Camino La Carrindanga km 7, 8000 Bahía Blanca, Argentina
[b] Departamento de Ingeniería Química, Universidad Nacional del Sur (UNS), Avda. Alem 1253, 8000 Bahía Blanca, Argentina

ARTICLE INFO

Article history:
Received 18 September 2017
Received in revised form 15 December 2017
Accepted 16 December 2017

Keywords:
Reverse atom transfer radical polymerization
Miniemulsion
Water-soluble initiator
Molecular weight distribution
Mathematical modeling

ABSTRACT

In this work, we study the reverse atom transfer radical polymerization in miniemulsion using a water-soluble initiator. This study is motivated by the technological advantages of performing polymerizations in dispersed systems, and the attractive possibilities of controlled radical polymerization techniques to produce tailor made polymers. A mathematical model for this system is presented. The model predicts average molecular properties as well as the full molecular weight distribution (MWD) for different experimental conditions. The method of moments is applied for calculating average properties and the probability generating function (pgf) technique is used to model the MWD. The model is based on the mass balance equations of the reacting species. It takes into account the reactions in both the aqueous and organic phases and the mass transfer between them. Predicted conversions, average molecular weights, polydispersity indexes and MWDs for different experimental conditions agree well with experimental data reported in the literature.

1. Introduction

Controlled radical polymerization (CRP) techniques have emerged as a promising field since they allow obtaining polymers with controlled molecular weights, low polydispersities, and defined architectures, employing mild reaction conditions. These techniques have been extensively studied in homogeneous systems, such as bulk and solution. However, over the last few years, there has been great interest in adapting these techniques to aqueous heterogeneous systems because they constitute a good alternative for large-scale production. The reasons are many: aqueous dispersed systems are environmentally friendly, show very good heat transfer, better process control, ease of mixing, flexibility, and ease of handling of the final product [1,2]. In fact, due to these advantages, many polymers currently obtained by conventional free-radical polymerization are produced in emulsion systems [1].

The application of CRP in dispersed systems has not been straightforward because it presents some complications, including partitioning of species between aqueous and organic phases, exit of radicals from polymer particles, poor colloidal stability, and interactions of species with other components of the recipe [1]. Despite these issues, different CRP techniques have been successfully applied in dispersed systems for several monomers and at different experimental conditions [3].

The first attempts to adapt CRP to aqueous dispersed systems were in emulsion. They were mostly unsuccessful because the emulsions did not present enough colloidal stability and had mass transfer limitations. Further studies focused on miniemulsions, where there is no need of diffusion of reactants through the aqueous phase from monomer droplets to micelles, as in emulsion systems. Miniemulsions are also able to host the polymerization of highly water insoluble monomers and to form particles containing additives such as dyes or pigments. [2,4]. Nevertheless, an hydrophobe of low molecular weight may need to be removed from the final latex, something that constitutes a disadvantage [1].

Atom transfer radical polymerization (ATRP) is one of the more widespread CRP techniques, together with nitroxide-mediated polymerization (NMP) and reversible addition–fragmentation chain transfer polymerization (RAFT). ATRP presents some distinct advantages over the others, such as the wide range of monomers it can polymerize, the commercial availability of reagents, the mild temperatures it employs and the capability of obtaining end-functionalized chains for subsequent reactions [5].

ATRP is based on the reversible equilibrium of a small number of radicals ($P_n^{\bullet}$) with a much larger number of dormant species (P_nBr) (Fig. 1). The dormant species react with a transition metal complex in its lower oxidation state ($CuBr_1/L$), which acts as an

* Corresponding author at: Planta Piloto de Ingeniería Química (PLAPIQUI), CONICET-UNS, Camino La Carrindanga km 7, 8000 Bahía Blanca, Argentina.
E-mail address: masteasuain@plapiqui.edu.ar (M. Asteasuain).

https://doi.org/10.1016/j.commatsci.2017.12.038
0927-0256/

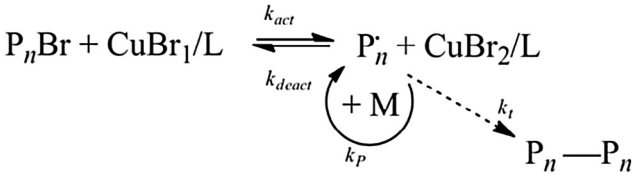

Fig. 1. Scheme of ATRP equilibrium.

activator, to produce the radicals and the transition metal complex in its higher oxidation state ($CuBr_2$/L), known as the deactivator. During this reaction, a halogen atom is transferred from the dormant species to the deactivator. The radicals may propagate incorporating more monomer units, terminate with other radicals or be deactivated again, regenerating the dormant species and the activator.

ATRP offers different procedures for initiating the reaction, as reported elsewhere [6]. One of these procedures is the reverse ATRP, in which the reaction begins with a conventional radical initiator (from which radicals $P_n^{\bullet}$ are generated) and the transition metal complex in its higher oxidation state. This procedure works well in aqueous dispersed systems since it employs Cu(II) complexes that are more tolerant to air than the Cu(I) complexes employed in direct ATRP [4]. Besides, it can employ many of the initiators used in conventional free-radical polymerization. Despite some disadvantages, such as relatively low initiation efficiency, reverse ATRP has demonstrated to be robust enough for obtaining polymers with controlled molecular weights and narrow molecular weight distributions in miniemulsion systems [7–9].

ATRP in miniemulsion has been extensively studied [2]. Considerable experimental research has been carried out employing several monomers (i.e. styrene, butyl acrylate, butyl methacrylate), varying the initiating procedure, the recipe and other experimental conditions (i.e. initiator, ligand, surfactant) [7,10,8,11]. Furthermore, theoretical work has been reported, employing deterministic as well as stochastic methods. For instance, Zetterlund et al. [11–15] studied extensively the compartmentalization effect in ATRP in dispersed systems using the modified Smith–Ewart equations. In addition, they investigated the effects of the partitioning of activator and deactivator, employing the software package Predici. At about the same time, Cunningham et al. [16] studied compartmentalization effects on polymerization rate and livingness of the reaction using the modified Smith–Ewart equations for a different system. They presented results on an average number of radicals per particle that indicate the system behaved as a bulk one for particles sized over 100 nm. Kagawa et al. [13] observed this behavior for particles larger than 70 nm for a similar system. On the other hand, Tobita [17–19] performed Monte Carlo simulations of ATRP in miniemulsion. He studied the effect of particle diameter on the kinetics and the role of segregation and fluctuation effects that are implicit in compartmentalized systems.

The studies reported so far have focused on phenomena present in ATRP in miniemulsion, such as compartmentalization and partitioning of components between phases, as well as their causes and how to exploit them to improve the process performance. To the best of our knowledge, a mathematical model able to predict accurately the molecular weight distribution has not been developed for this system.

In the above context, this work aims at developing a mathematical tool to predict the main molecular properties of the product obtained through a reverse ATRP in miniemulsion using a water-soluble initiator. The user of this tool would be able to calculate the molecular characteristics of the final polymer, given a certain polymerization recipe. The model we present in this work predicts average molecular properties, such as number and weight average molecular weights, as well as the full molecular weight distribution (MWD) for different experimental conditions. It is applicable to systems with particle sizes large enough for compartmentalization effects to be negligible. It is based on the mass balance equations of the reacting species. The method of moments was applied for calculating average properties and the probability generating function (pgf) technique is used to model the MWD. Parameter estimation was performed to fit the values of several model parameters, employing experimental data available in the literature [7].

2. Mathematical model

A mathematical model of the reverse ATRP in miniemulsion initiated by a water-soluble initiator is developed based on the mass balance equations of the reacting species. It takes into account the reactions in both the aqueous and organic phases, as well as the mass transfer between them.

2.1. Description of the heterogeneous system

In order to understand the mechanisms and phenomena involved, the system is described first.

The miniemulsion consists of an organic phase, composed of the monomer dispersed as droplets in a continuous aqueous phase. The monomer is also partially dissolved in the aqueous phase. The initial composition of the miniemulsion includes the water-soluble initiator present in the aqueous phase, and a deactivator dissolved in both the organic and aqueous phases. For the sake of clarity, $CuBr_2$/L will be taken as an example of a usual deactivator in the remainder of the paper without losing model generality. The distribution of the reacting species in the miniemulsion is shown in Fig. 2.

The water-soluble initiator decomposes in the aqueous phase, generating radicals. These radicals may react with other species present in the aqueous phase: with the monomer in the propagation reaction or the transfer to monomer reaction, with other radicals in termination reactions, or with deactivator $CuBr_2$/L. The latter reaction generates dormant species as well as the activator $CuBr_1$/L. The activator and the dormant species can react with each other in the reverse reaction, establishing the ATRP equilibrium in the water phase. If the radicals propagate, they grow until they reach a chain length that renders them hydrophobic, or surface-active. At the same time, dormant species also become hydrophobic when they reach a given chain length. It is considered that as soon as these species achieve hydrophobicity, they irreversibly enter the organic phase, where they may be deactivated (radicals)

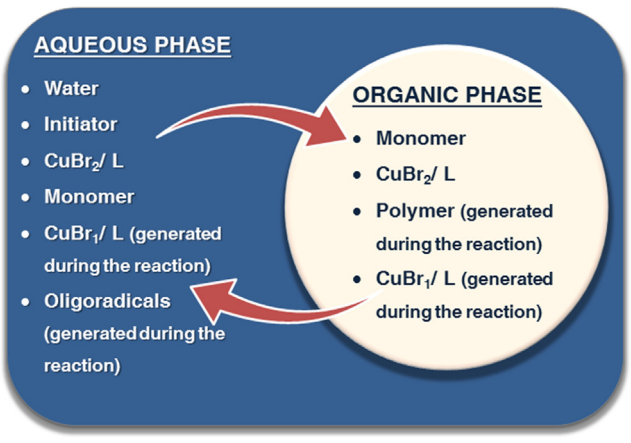

Fig. 2. Distribution of reacting species in the heterogeneous system.

or activated (dormant species) by the deactivator $CuBr_2$/L or activator $CuBr_1$/L, respectively, establishing the ATRP equilibrium in the organic phase. All radicals in this phase can also participate in propagation, termination or transfer to monomer reactions.

The following assumptions are adopted in the development of our model of the miniemulsion system:

i. The phase volumes are constant.
ii. Droplets are larger than 100 nm. For this reason, compartmentalization effects are negligible [13,16].
iii. The monomer, activator, and deactivator are partitioned between both phases. Mass equilibrium between the phases is reached rapidly and maintained throughout the polymerization. This assumption is in agreement with statements made in other theoretical works for direct ATRP and NMP in miniemulsion [11,20].
iv. The aqueous phase is saturated with monomer [21].
v. All of the water-soluble initiator is in the aqueous phase.
vi. Oligoradicals up to a finite chain length are water-soluble. Longer radicals are hydrophobic [7,21]. The same is assumed for dormant species [20]. Oligoradicals and dormant species may only enter the organic droplets; exit and reentry of these species are neglected [22].
vii. The surfactant and costabilizer (components needed to carry out the reaction in miniemulsion) do not interfere with any reactants [21].

Assumptions iii and vi are discussed in the next sections.

2.2. Kinetic mechanism

The kinetic mechanism considered for this work is reported in Table 1.

The chemical species involved are: initiator (I-I), initiation radical ($I^{\bullet}$), initiation radical in dormant state (IBr), monomer (M), radicals with n monomer units ($P_n^{\bullet}$), dormant species with n monomer units (P_nBr), terminated (dead) polymer chains with n monomer units (D_n), activator ($CuBr_1$/L) and deactivator ($CuBr_2$/L). The subscripts *aq* and *org* indicate whether the species belong to the aqueous or organic phase, respectively. The subscripts θ and $(\theta - 1)$ represent the critical degree of polymerization for which radicals and dormant species respectively, become hydrophobic and enter the organic phase. For each reaction, the corresponding kinetic rate constant is identified with the letter k, with an appropriate subscript. The efficiency of the initiator decomposition reaction is accounted for by "f".

An average propagation rate constant with respect to chain length ($\langle k_P \rangle$) is employed in the model. However, previous studies have demonstrated that k_P has a chain length-dependency in the short chain-length region [26,27]. In consequence, larger propagation constants are used for radicals with one and two monomer units (k_{P1}, k_{P2}). These constants are employed in the aqueous phase where these oligoradicals predominate.

In the case of the organic phase, the model takes into account the chain-length dependency of the termination rate constant (k_t), a phenomenon that has been widely studied. In this work, we will focus on the ATRP of n-Butyl Methacrylate (n-BMA), as a case study. Buback et al. [28] found a dependence of k_t with monomer conversion in the free radical bulk polymerization of this monomer. This dependence is characterized by an initial plateau region (due to segmental diffusion) up to monomer conversions of 25–30%, followed by a decrease at higher conversions (due to translational diffusion and then reaction diffusion control). In the present work, we approximated the equation used by Buback et al. [28] by a piecewise function, depicted in Fig. 3. In order to improve the numerical behavior of the optimization solver used for the estimation of the model parameters, this piecewise dependency is implemented in the model by a smoothing function with continuous derivatives, as shown in Eq. (17):

$$k_t(X) = \{1 - 0.5 \cdot [\tanh(5 \cdot (X - 25)) + 1]\} \cdot 1 \cdot 10^7 + 0.5 \cdot [\tanh(5 \cdot (X - 25)) + 1] \cdot (1.3 \cdot 10^7 - 1.2 \cdot 10^5 \cdot X) \ (L\ mol^{-1}\ s^{-1}) \quad (17)$$

where X represents de monomer conversion. The function in Eq. (17) coincides almost exactly with the piecewise function. As may be observed in Fig. 3, the discrepancy is only noticeable around 25% conversion, where the largest error is 0.033%.

For the aqueous phase, it is not necessary to take into account the dependence of k_t with conversion because only small species are located there. In that phase, a termination rate constant (k_{td_aq}, k_{tc_aq}) close to the diffusion limit is employed (10^9 L mol^{-1} s^{-1}) according to the values reported elsewhere for aqueous systems of similar characteristics [22].

2.3. Species entry to the organic phase

The primary radicals generated in the aqueous phase are not hydrophobic enough to enter the organic phase; they need to add a few monomer units first. Maxwell et al. [22] proposed that irreversible radical capture by organic droplets is instantaneous for oligoradicals of degree of polymerization θ, where θ is a small integer. Thus, oligoradicals with degrees of polymerization greater than or equal to θ enter the organic phase instantaneously and irreversibly. For simplicity, we assume that all entering oligoradicals are of size θ.

Maxwell et al. [22] proposed the expression shown in Eq. (18) for estimating this value. They obtained this formula for a persulfate-initiated system, but it can be applied for other initiators since the dependence of θ with the type of initiator is expected to be low [22].

$$\theta = 1 + \mathrm{int}\left(\frac{23[\mathrm{kJ\ mol^{-1}}]}{RT \ln([M_{aq,sat}])}\right) \quad (18)$$

In this expression, function int(.) rounds off the quantity in parentheses to the lower integer value, R is the ideal gas constant and $[M_{aq,sat}]$ is the saturation molar concentration of the monomer in water at the reaction temperature T.

As previously discussed, it is considered that all radicals with θ monomer units enter the organic phase instantaneously as soon as they are formed (Eq. (12)). Therefore, there are no radicals of chain length θ in the aqueous phase, and the rate of entry of these radicals into the organic phase equals their rate of generation. For this reason, the oligoradical entry is represented in the model by Eq. (19).

$$\textit{Rate of oligoradicals entry} = k_{P(\theta-1)}[M]_{aq}[P^{\bullet}_{(\theta-1)}]_{aq}V_{aq} \quad (19)$$

where $[M]_{aq}$ is the monomer concentration in the aqueous phase, $[P^{\bullet}_{\theta-1}]_{aq}$ is the concentration of radicals with $(\theta - 1)$ monomer units in this phase and V_{aq} is the volume of the aqueous phase.

On the other hand, it is also considered that any dormant species with $(\theta - 1)$ monomer units acts as an oligoradical of θ units. This is based on the assumption that the halogen atom is similar to one monomer unit [20]. As in the case of oligoradicals, they enter the organic phase instantaneously as soon as they are formed (Eq. (13)), so there are no dormant species of chain length $(\theta - 1)$ in the aqueous phase, and their rate of entry into the organic phase equals their generation rate. This is represented as follows:

$$\textit{Rate of dormant species entry} = k_{deact}[CuBr_2/L]_{aq}[P^{\bullet}_{\theta-1}]_{aq}V_{aq} \quad (20)$$

Table 1
Kinetic mechanism of the reverse ATRP in miniemulsion initiated by a water-soluble initiator.

Reaction	Equation	Ref
Initiator decomposition (aqueous phase)	$I - I \xrightarrow{k_{df}} 2I^{\bullet}$ (1)	[7,21,23,24,25]
Initiation (aqueous phase)	$I^{\bullet} + M \xrightarrow{k_i} P_1^{\bullet}$ (2)	
Propagation (aqueous phase)	$P_1^{\bullet} + M \xrightarrow{k_{p1}} P_2^{\bullet}$ (3)	
	$P_2^{\bullet} + M \xrightarrow{k_{p2}} P_3^{\bullet}$ (4)	
	$P_n^{\bullet} + M \xrightarrow{\langle k_p \rangle} P_{n+1}^{\bullet} \quad n = 3, \ldots, \theta - 1$ (5)	
Propagation (organic phase)	$P_n^{\bullet} + M \xrightarrow{\langle k_p \rangle} P_{n+1}^{\bullet}$ (6)	
Termination (aqueous and organic phases) By disproportionation	$P_n^{\bullet} + P_m^{\bullet} \xrightarrow{k_{td-aq}/k_{td-org}} D_n + D_m$ (7)	
By combination	$P_n^{\bullet} + P_m^{\bullet} \xrightarrow{k_{td-aq}/k_{td-org}} D_n + D_m$ (8)	
ATRP equilibrium (aqueous and organic phases)	$IBr + CuBr_1/L \underset{k_{deact}}{\overset{k_{act}}{\rightleftarrows}} I^{\bullet} + CuBr_2/L$ (9)	
	$P_nBr + CuBr_1/L \underset{k_{deact}}{\overset{k_{act}}{\rightleftarrows}} P_n^{\bullet} + CuBr_2/L$ (10)	
Chain transfer to monomer (aqueous and organic phases)	$P_n^{\bullet} + M \xrightarrow{k_{trm}} D_n + P_1^{\bullet}$ (11)	
Oligoradicals entry (aqueous-organic interface)	$P_{0aq}^{\bullet} \rightarrow P_{0org}^{\bullet}$ (12)	[4,22]
Dormant species entry (aqueous-organic interface)	$P_{(\theta-1)}Br_{aq} \rightarrow P_{(\theta-1)}Br_{org}$ (13)	[20]
Partitioning of $CuBr_1/L$, $CuBr_2/L$ and monomer (aqueous-organic interface)	$CuBr_1/L_{aq} \underset{k_2}{\overset{k_1}{\rightleftarrows}} CuBr_1/L_{org}$ (14)	[21,20]
	$CuBr_2/L_{aq} \underset{k_4}{\overset{k_3}{\rightleftarrows}} CuBr_2/L_{org}$ (15)	
	$M_{aq} \underset{k_6}{\overset{k_5}{\rightleftarrows}} M_{org}$ (16)	

where $[CuBr_2/L]_{aq}$ is the deactivator concentration in the aqueous phase.

2.4. Partitioning of species

Partitioning of several species occurs in heterogeneous systems. This work considers the partitioning of the deactivator ($CuBr_2/L$), activator ($CuBr_1/L$) and monomer between the organic and aqueous phases.

The partitioning depends on the total concentration of the species as well as on the temperature [21]. It is represented by using partition coefficients γ_i which are defined as [21]

$$\gamma_i = \frac{[\mathrm{i}]_{org}}{[\mathrm{i}]_{aq}} \tag{21}$$

where $[i]_j$ represents the concentration of species i in phase j, j = *org*, *aq*.

As previously discussed it is considered that phase equilibrium is maintained throughout the reaction due to a fast mass transfer between phases. This implies that the rates of the forward and reverse mass transfer reactions are approximately equal, i.e.:

$$-k_{forward}[\mathrm{i}]_{aq}\mathrm{V}_{aq} + k_{reverse}[\mathrm{i}]_{org}\mathrm{V}_{org} \approx 0 \tag{22}$$

Combination of Eq. (21) and Eq. (22) leads to the following relationship between the transfer rate coefficients and the partition coefficient:

$$\frac{k_{forward}}{k_{reverse}} = \frac{[\mathrm{i}]_{org}}{[\mathrm{i}]_{aq}}\frac{\mathrm{V}_{org}}{\mathrm{V}_{aq}} = \gamma_i \frac{\mathrm{V}_{org}}{\mathrm{V}_{aq}} \tag{23}$$

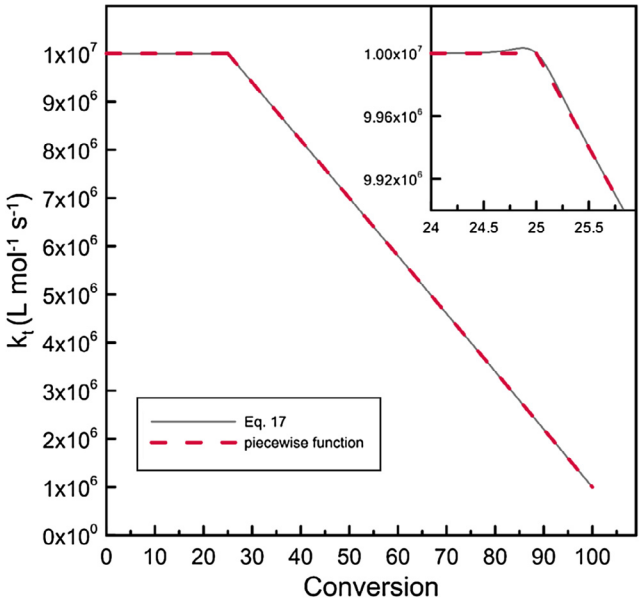

Fig. 3. Termination rate coefficient vs monomer conversion. The insert shows an amplification of the graph around 25% conversion.

where $k_{forward}/k_{reverse}$ corresponds to k_1/k_2, k_3/k_4 or k_5/k_6 for the kinetic mechanism shown in Table 1.

The pseudo-equilibrium between the species in the aqueous and organic phases represented by Eq. (22) can be achieved in a numerical simulation by assigning large values (>10^8 s^{-1}) to the forward and reverse transfer rate coefficients.[20] Therefore, in this work large values, in the order of 10^8–10^9 s^{-1}, are given to the reverse transfer coefficients, and the forward coefficients are determined from Eq. (23).

2.5. Partitioning of $CuBr_2$/L and $CuBr_1$/L

A correct estimation of the partitioning of $CuBr_2$/L and $CuBr_1$/L is essential since these species are key components of the ATRP equilibrium. The activator $CuBr_1$/L is more soluble in the organic phase than the deactivator $CuBr_2$/L. Therefore, the partition coefficient of $CuBr_1$/L should be larger than that of $CuBr_2$/L. Qiu et al. [21] measured the partition coefficients for these two species, but with a more hydrophilic ligand than the one considered in this work. In consequence, it is expected that the partition coefficients of this system are larger than the ones reported by Qiu et al. [21] Anyway, the reported values are taken as a reference in the present work since they are used as a starting guess for the estimation of these parameters. More details are presented in Section 4.

2.6. Partitioning of monomer

No information was found in the literature about the partition of the monomer for this system. Hence, this parameter is calculated using Eq. (21). Concentrations of monomer in the aqueous and organic phases are estimated as follows: first, it is assumed that the aqueous phase is saturated with monomer, and therefore $[M]_{aq} = [M]_{aq,sat}$. Then, the monomer concentration in the organic phase is calculated as shown below:

$$\text{monomer moles}_{aq} = [M]_{aq,sat} V_{aq} \tag{24}$$

$$\text{monomer moles}_{org} = \text{total moles} - \text{monomer moles}_{aq} \tag{25}$$

$$[M]_{org} = \frac{\text{monomer moles}_{org}}{V_{org}} \tag{26}$$

From Eq. (21), the monomer partition coefficient is:

$$\gamma_M = \frac{[M]_{org}}{[M]_{aq}} \tag{27}$$

2.7. Modeling of average molecular properties and MWD

Since the system consists of two phases, the species present in both of them are considered as two different entities for mathematical treatment. Species concentrations are evaluated relative to the volume of the phase in which they are located.

The molar balance equations of the species present in the reacting system are reported below. A batch reactor is assumed.

Initiator

$$\frac{d([I-I]V_{aq})}{dt} = -k_d[I-I]V_{aq} \tag{28}$$

$$\frac{d([I^\bullet]V_{aq})}{dt} = 2fk_d[I-I]V_{aq} - k_i[M]_{aq}[I^\bullet]V_{aq} - k_{deact}[CuBr_2/L]_{aq}[I^\bullet]V_{aq} + k_{act}[CuBr_1/L]_{aq}[IBr]V_{aq} \tag{29}$$

$$\frac{d([IBr]V_{aq})}{dt} = k_{deact}[CuBr_2/L]_{aq}[I^\bullet]V_{aq} - k_{act}[CuBr_1/L]_{aq}[IBr]V_{aq} \tag{30}$$

Monomer

$$\frac{d([M]_{aq}V_{aq})}{dt} = -k_i[M]_{aq}[I^\bullet]V_{aq} - k_{P1}[M]_{aq}[P_1^\bullet]_{aq}V_{aq} - k_{P2}[M]_{aq}[P_2^\bullet]_{aq}V_{aq} - \langle k_P\rangle[M]_{aq}\sum_{n=3}^{\theta-1}[P_n^\bullet]_{aq}V_{aq} - k_{trm}[M]_{aq}\sum_{n=1}^{\theta-1}[P_n^\bullet]_{aq}V_{aq} - k_5[M]_{aq}V_{aq} + k_6[M]_{org}V_{org} \tag{31}$$

$$\frac{d([M]_{org}V_{org})}{dt} = -\langle k_P\rangle[M]_{org}\left(\sum_{n=1}^{\infty}[P_n^\bullet]_{org}\right)V_{org} - k_{trm}[M]_{org}\left(\sum_{n=1}^{\infty}[P_n^\bullet]_{org}\right)V_{org} + k_5[M]_{aq}V_{aq} - k_6[M]_{org}V_{org} \tag{32}$$

Activator

$$\frac{d([CuBr_1/L]_{aq}V_{aq})}{dt} = k_{deact}[CuBr_2/L]_{aq}\left([I^\bullet] + \sum_{n=1}^{\theta-1}[P_n^\bullet]_{aq}\right)V_{aq} - k_{act}[CuBr_1/L]_{aq}\left([IBr] + \sum_{n=1}^{\theta-2}[P_nBr]_{aq}\right)V_{aq} - k_1[CuBr_1/L]_{aq}V_{aq} + k_2[CuBr_1/L]_{org}V_{org} \tag{33}$$

$$\frac{d([CuBr_1/L]_{org}V_{org})}{dt} = k_{deact}[CuBr_2/L]_{org}\left(\sum_{n=1}^{\infty}[P_n^\bullet]_{org}\right)V_{org} - k_{act}[CuBr_1/L]_{org}\left(\sum_{n=1}^{\infty}[P_nBr]_{org}\right)V_{org} + k_1[CuBr_1/L]_{aq}V_{aq} - k_2[CuBr_1/L]_{org}V_{org} \tag{34}$$

Deactivator

$$\frac{d([CuBr_2/L]_{aq}V_{aq})}{dt} = -k_{deact}[CuBr_2/L]_{aq}\left([I^\bullet] + \sum_{n=1}^{\theta-1}[P_n^\bullet]_{aq}\right)V_{aq} + k_{act}[CuBr_1/L]_{aq}\left([IBr] + \sum_{n=1}^{\theta-2}[P_nBr]_{aq}\right)V_{aq} - k_3[CuBr_2/L]_{aq}V_{aq} + k_4[CuBr_2/L]_{org}V_{org} \quad (35)$$

$$\frac{d([CuBr_2/L]_{org}V_{org})}{dt} = -k_{deact}[CuBr_2/L]_{org}\left(\sum_{n=1}^{\infty}[P_n^\bullet]_{org}\right)V_{org} + k_{act}[CuBr_1/L]_{org}\left(\sum_{n=1}^{\infty}[P_nBr]_{org}\right)V_{org} + k_3[CuBr_2/L]_{aq}V_{aq} - k_4[CuBr_2/L]_{org}V_{org} \quad (36)$$

Radicals with n monomer units-Aqueous phase (n = 1,. . .,(θ − 1))

$$\frac{d([P_n^\bullet]_{aq}V_{aq})}{dt} = k_i[M]_{aq}[I^\bullet]V_{aq}\delta_{n,1} - k_{Pn}[M]_{aq}[P_n^\bullet]_{aq}V_{aq} + k_{Pn-1}[M]_{aq}[P_{n-1}^\bullet]_{aq}V_{aq}(1-\delta_{n,1}) - \left[(k_{td\_aq}+k_{tc\_aq})[P_n^\bullet]_{aq}\left(\sum_{m=1}^{\theta-1}[P_m^\bullet]_{aq}\right)V_{aq}\right] - k_{deact}[CuBr_2/L]_{aq}[P_n^\bullet]_{aq}V_{aq} + k_{act}[CuBr_1/L]_{aq}[P_nBr]_{aq}V_{aq}(1-\delta_{n,\theta-1}) + k_{trm}[M]_{aq}\left(\sum_{m=1}^{\theta-1}[P_m^\bullet]_{aq}\right)V_{aq}\delta_{n,1} - k_{trm}[M]_{aq}[P_n^\bullet]_{aq}V_{aq} \quad (37)$$

where $\delta_{n,i}$ is the Kronecker delta ($\delta_{n,i} = 1$ if $n = i$, $\delta_{n,i} = 0$ otherwise).

As explained above, we consider that all oligoradicals with length $n = \theta$ from the aqueous phase, enter instantaneously the organic phase as soon as they are formed. Thus, their concentration in the aqueous phase is zero, and the rate of entry of this species into the organic phase is equal to its rate of generation in the aqueous phase, as expressed in Eq. (19).

Radicals with n monomer units-Organic phase

$$\frac{d([P_n^\bullet]_{org}V_{org})}{dt} = -\langle k_P\rangle[M]_{org}[P_n^\bullet]_{org}V_{org} + \langle k_P\rangle[M]_{org}[P_{n-1}^\bullet]_{org}V_{org}(1-\delta_{n,1}) - (k_{td\_org}+k_{tc\_org})[P_n^\bullet]_{org}\left(\sum_{m=1}^{\infty}[P_m^\bullet]_{org}\right)V_{org} - k_{deact}[CuBr_2/L]_{org}[P_n^\bullet]_{org}V_{org} + k_{act}[CuBr_1/L]_{org}[P_nBr]_{org}V_{org} - k_{trm}[M]_{org}[P_n^\bullet]_{org}V_{org} + k_{trm}[M]_{org}\left(\sum_{m=1}^{\infty}[P_m^\bullet]_{org}\right)V_{org}\delta_{n,1} + k_{P(\theta-1)}[M]_{aq}[P_{\theta-1}^\bullet]_{aq}V_{aq}\delta_{n,\theta} \quad (38)$$

where the last term corresponds to the rate of entry of radicals of chain length θ into the organic phase.

Dormant species with n monomer units-Aqueous phase (n = 1,. . .,(θ − 2))

$$\frac{d([P_nBr]_{aq}V_{aq})}{dt} = k_{deact}[CuBr_2/L]_{aq}[P_n^\bullet]_{aq}V_{aq} - k_{act}[CuBr_1/L]_{aq}[P_nBr]_{aq}V_{aq} \quad (39)$$

Note that we consider that all dormant species with length n = θ − 1 in the aqueous phase, enter instantaneously the organic phase as soon as they are formed. Thus, their concentration in the aqueous phase is zero, and the rate of entry of this species into the organic phase is equal to its rate of generation in the aqueous phase, as expressed in Eq. (20).

Dormant species with n monomer units-Organic phase

$$\frac{d([P_nBr]_{org}V_{org})}{dt} = k_{deact}[CuBr_2/L]_{org}[P_n^\bullet]_{org}V_{org} - k_{act}[CuBr_1/L]_{org}[P_nBr]_{org}V_{org} + k_{deact}[CuBr_2/L]_{aq}[P_{\theta-1}^\bullet]_{aq}V_{aq}\delta_{n,\theta-1} \quad (40)$$

where the last term corresponds to the rate of entry of dormant species of chain length $(\theta - 1)$ into the organic phase.

Dead polymer chains with n monomer units – Aqueous Phase (n = 1,. . .,2(θ − 1))

$$\frac{d([D_n]_{aq}V_{aq})}{dt} = k_{td\_aq}[P_n^\bullet]_{aq}\left(\sum_{m=1}^{\theta-1}[P_m^\bullet]_{aq}\right)V_{aq}\left(\sum_{m=1}^{\theta-1}\delta_{n,m}\right) + \frac{1}{2}k_{tc\_aq}\left(\sum_{r=1}^{n-1}[P_r^\bullet]_{aq}[P_{n-r}^\bullet]_{aq}\right)V_{aq}(1-\delta_{n,1}) + k_{trm}[M]_{aq}[P_n^\bullet]_{aq}V_{aq}\left(\sum_{m=1}^{\theta-1}\delta_{n,m}\right) \quad (41)$$

Dead polymer chains with n monomer units – Organic Phase

$$\frac{d([D_n]_{org}V_{org})}{dt} = k_{td\_org}[P_n^\bullet]_{org}\left(\sum_{m=1}^{\infty}[P_m^\bullet]_{org}\right)V_{org} + \frac{1}{2}k_{tc\_org}\left(\sum_{r=1}^{n-1}[P_r^\bullet]_{org}[P_{n-r}^\bullet]_{org}\right)V_{org}(1-\delta_{n,1}) + k_{trm}[M]_{org}[P_n^\bullet]_{org}V_{org} \quad (42)$$

The average molecular properties are calculated through the well-known method of moments. We apply this method to the mass balances of the radical, dormant and dead polymer chains of the organic phase and obtain the moment balance equations. The moments used and their corresponding balances are shown below:

Moment of order a (a = 0, 1 or 2) of radicals $\lambda_a = \sum_{n=1}^{\infty}n^a[P_n^\bullet]_{org}$

$$\frac{d(\lambda_aV_{org})}{dt} = -\langle k_P\rangle[M]_{org}\lambda_aV_{org} + \langle k_P\rangle[M]_{org}\sum_{j=0}^{a}\binom{a}{j}\lambda_jV_{org} - (k_{td\_org}+k_{tc\_org})\lambda_a\lambda_0V_{org} - k_{deact}[CuBr_2/L]_{org}\lambda_aV_{org} + k_{act}[CuBr_1/L]_{org}\mu_aV_{org} - k_{trm}[M]_{org}\lambda_aV_{org} + k_{trm}[M]_{org}\lambda_0V_{org} + k_{P(\theta-1)}[M]_{aq}[P_{\theta-1}^\bullet]_{aq}V_{aq}\theta^a \quad (43)$$

Moment of order a (a = 0, 1 or 2) of dormant species $\mu_a = \sum_{n=1}^{\infty}n^a[P_nBr]_{org}$

$$\frac{d(\mu_aV_{org})}{dt} = k_{deact}[CuBr_2/L]_{org}\lambda_aV_{org} - k_{act}[CuBr_1/L]_{org}\mu_aV_{org} + k_{deact}[CuBr_2/L]_{aq}[P_{\theta-1}^\bullet]_{aq}V_{aq}(\theta-1)^a \quad (44)$$

Moment of order a (a = 0, 1 or 2) of dead polymer chains $\varepsilon_a = \sum_{n=1}^{\infty}n^a[D_n]_{org}$

$$\frac{d(\varepsilon_aV_{org})}{dt} = k_{td\_org}\lambda_0\lambda_aV_{org} + \frac{1}{2}k_{tc\_org}\sum_{j=0}^{a}\binom{a}{j}\lambda_j\lambda_{a-j}V_{org} + k_{trm}[M]_{org}\lambda_aV_{org} \quad (45)$$

Note that moments of order 0 of radical and dormant chains appear in Eqs. (32), (34), (36), (38) and (42).

The number and weight average molecular weights are calculated from the moments of order 0, 1 and 2 according to:

$$\overline{M_n} = \frac{(\lambda_1 + \mu_1 + \varepsilon_1)}{(\lambda_0 + \mu_0 + \varepsilon_0)} M_{w,M} \tag{46}$$

$$\overline{M_w} = \frac{(\lambda_2 + \mu_2 + \varepsilon_2)}{(\lambda_1 + \mu_1 + \varepsilon_1)} M_{w,M} \tag{47}$$

where $M_{w,M}$ is the molecular weight of the monomer. Additionally, the polydispersity index is defined as:

$$\mathrm{PDI} = \frac{\overline{M_w}}{\overline{M_n}} \tag{48}$$

A complete characterization of the polymer requires computing the full molecular weight distribution. Direct solution of Eqs. (38), (40) and (42) for $n = 1, \ldots, \infty$ would yield the chain length distributions $[P_n^*]_{org}$ vs n, $[P_nBr]_{org}$ vs n and $[D_n]_{org}$ vs n, from which the MWD of all polymeric species (i.e. $[P_n^*]_{org}$ + $[P_nBr]_{org}$ + $[D_n]_{org}$) can be calculated. In this work, equations (38), (40) and (42) are not solved directly because there are more efficient ways of obtaining these distributions. Even though the infinity limit on n could be replaced by a suitable upper bound n_{max}, the resulting number of equations would still be very large. Here, the MWD is modeled using the probability generating function (pgf) technique. This method consists of transforming the molar balances of the different polymer species into the pgf domain, providing balance equations for the pgf transform of the MWD [29]. After solving these balances, the entire molecular weight distribution is recovered using an appropriate inversion method [30]. The pgf technique has been successfully used in our group to predict MWDs in several polymerization systems at laboratory an industrial scales [29–33]. It has the advantage of not requiring previous knowledge of the shape of the MWD. It is easy to implement even for non-expert users by resorting to the use of published Transform Tables [29], resulting in equation systems that can be solved in standard desktop computers in a reasonable time.

Briefly, the pgf is defined as:

$$\phi_a(z) = \sum_{n=0}^{\infty} z^n n^a \frac{[X_n]}{\psi_a} \tag{49}$$

where ϕ_a is the pgf of order a of the distribution function $[X_n]$, X is any of the polymer species, ψ_a is the moment of order a of $[X_n]$ and z is the dummy variable of the pgf. In what follows we name the pgf of species $P_n^\bullet$, P_nBr and D_n as σ_a, φ_a and ϑ_a, respectively.

Applying the pgf transformation to the molar balances of the polymer species, the following pgf balances are obtained:

Pgf of order zero of radicals ($\sigma_0(z)$):

$$\begin{aligned}\frac{d(\lambda_0\sigma_0(z)V_{org})}{dt} = &-\langle k_P\rangle [M]_{org}(\lambda_0\sigma_0(z))V_{org} \\ &+ \langle k_P\rangle [M]_{org} z(\lambda_0\sigma_0(z))V_{org} - (k_{td\_org} \\ &+ k_{tc\_org})\lambda_0(\lambda_0\sigma_0(z))V_{org} \\ &- k_{deact}[CuBr_2/L]_{org}(\lambda_0\sigma_0(z))V_{org} \\ &+ k_{act}[CuBr_1/L]_{org}(\mu_0\varphi_0(z))V_{org} \\ &- k_{trm}[M]_{org}(\lambda_0\sigma_0(z))V_{org} \\ &+ k_{trm}[M]_{org}\lambda_0 z V_{org} \\ &+ k_{P(\theta-1)}[M]_{aq}[P^\bullet_{\theta-1}]_{aq}V_{aq}z^\theta \end{aligned} \tag{50}$$

Pgf of order zero of dormant species ($\varphi_0(z)$):

$$\begin{aligned}\frac{d(\mu_0\varphi_0(z)V_{org})}{dt} = &\, k_{deact}[CuBr_2/L]_{org}(\lambda_0\sigma_0(z))V_{org} \\ &- k_{act}[CuBr_1/L]_{org}(\mu_0\varphi_0(z))V_{org} \\ &+ k_{deact}[CuBr_2/L]_{aq}[P^\bullet_{\theta-1}]_{aq}V_{aq}z^{\theta-1}\end{aligned} \tag{51}$$

Pgf of order zero of dead polymer chains ($\vartheta_0(z)$):

$$\begin{aligned}\frac{d(\varepsilon_0\vartheta_0(z)V_{org})}{dt} = &\, k_{td\_org}\lambda_0(\lambda_0\sigma_0(z))V_{org} \\ &+ \frac{1}{2}k_{tc\_org}(\lambda_0\sigma_0(z))^2V_{org} \\ &+ k_{trm}[M]_{org}(\lambda_0\sigma_0(z))V_{org}\end{aligned} \tag{52}$$

Pgf of all chains forming the polymer (radicals, dormant species and dead polymer chains):

$$\Omega_0(z) = \frac{\lambda_0\sigma_0(z) + \mu_0\varphi_0(z) + \varepsilon_0\vartheta_0(z)}{\lambda_0 + \mu_0 + \varepsilon_0} \tag{53}$$

The full MWD of the sum of all polymer chains (i.e. radical, dormant and dead chains) is obtained from the inversion of $\Omega_0(z)$ [30].

It is noteworthy that the pgf balances are solved for the product of moment times the pgf, but not for the pgf variable alone. This has the advantage of avoiding indeterminations whenever the species concentration is zero. Since the moments are calculated independently from the pgf balances, the pgf values may be easily obtained from the calculated product mentioned above.

In order to limit the size of this system we only use pgf of order zero. With these pgfs, we obtain the MWD expressed in number fraction [29]. The weight fraction MWD is obtained from the latter. It is important to highlight that no prior knowledge of the shape of the MWD or any simplifying assumptions is required. Additionally, the model has a manageable size for modern computational resources (6627 differential equations, 13272 algebraic equations) and can be solved in a reasonable time (CPU time of 45–70 s for the different experiments on standard i5 Intel® desktop computer).

The equations to be solved are Eqs. (28)–(37), (39), (41), (43)–(48), (50)–(53). Initial conditions of the mass balances of initiator, monomer in aqueous and organic phase, and activator and deactivator in aqueous and organic phases vary with the different experiments and are named $[I]_0$, $[M]_{aq,0}$, $[M]_{org,0}$, $[CuBr_1/L]_{aq,0}$, $[CuBr_1/L]_{org,0}$, $[CuBr_2/L]_{aq,0}$ and $[CuBr_2/L]_{org,0}$, respectively. Initial conditions for moment balances, pgf balances and the remaining species are equal to zero. The model also requires the values of the kinetic constants. Most of them were taken from the literature, but others were estimated as described next.

Simulations and the parameter estimation were performed in gPROMS (Process Systems Enterprise, Ltd.). Simulations employed the built-in solver DASOLV, while the parameter estimation was solved using the Parameter Estimation entity of gPROMS. A standard desktop computer is used with an Intel® Core™ i5-4460 3.20 GHz processor and 8 GB of RAM memory.

3. Experimental data

The parameter estimation was carried out using experimental data from the literature [7]. The experimental system consisted of a reverse ATRP in miniemulsion initiated by a water soluble radical initiator in a batch reactor at 70 °C. The monomer was n-butyl methacrylate (n-BMA), the deactivator/ligand was $CuBr_2$/EH_6TREN and the initiator was 2,2′-azobis[2-(2-imidazolin-2-yl)propane] dihydrochloride (VA-044). The corresponding recipes are summarized in Table 2.

For each experiment, Matyjaszewski et al. [7] reported measurements of conversion, $\overline{M_n}$ and PDI at different reaction times. In addition, the MWDs for experiment 400/1/1 at four conversions (39.4%, 60%, 85% and 98.8%) were presented. Please note that the particle sizes reported for these experiments were in the range of 200–250 nm.

Table 2
Experiments employed in parameter estimation.

Experiment[a]	$[I]_{aq,0}$ (mmol/L)	$[M]_{aq,0}$ (mmol/L)	$[M]_{org,0}$ (mol/L)	$[CuBr_2/L]_{aq,0}$ (mmol/L)	$[CuBr_2/L]_{org,0}$ (mmol/L)	$[CuBr_2/L]_0$[b] (mmol/L)
200/1/1	8.6	3.4	6.9	1.1	30.2	34.6
400/1/1	4.3	3.4	6.9	0.9	13.7	17.3
800/1/1	2.2	3.4	6.9	0.7	5.8	8.6
400/1.5/1	4.3	3.4	6.9	0.8	22.7	25.9
800/2/1	2.2	3.4	6.9	0.9	13.7	17.3

$[CuBr_1/L]_{aq,0} = [CuBr_1/L]_{org,0}=0$.
Organic phase volume = 5 cm^3.
Aqueous phase volume = 20 cm^3.
Monomer molecular weight = 142.2 g/mol.
[a] The code employed corresponds to the total ratio of equivalents M/$CuBr_2$/I used in each experiment.
[b] Total concentration of $CuBr_2$ relative to the organic phase volume (before mixing with water).

Table 3
Model parameters at 70 °C.

Symbol	Value	Ref.
k_d	7.70×10^{-4} (s^{-1})	[7]
f	1	[7]
k_i	1×10^9 (L mol^{-1} s^{-1})	[20,22]
$\langle k_p \rangle$	1243 (L mol^{-1} s^{-1})	[34]
k_{P1}	27,690 (L mol^{-1} s^{-1})	This work
k_{P2}	23,924 (L mol^{-1} s^{-1})	This work
k_{td_org}	$0.9k_{t\_org}$ (L mol^{-1} s^{-1})	[23]
k_{td_aq}	$0.9k_{t\_aq}$ (L mol^{-1} s^{-1})	
k_{tc_org}	$0.1k_{t\_org}$ (L mol^{-1} s^{-1})	[23]
k_{tc_aq}	$0.1k_{t\_aq}$ (L mol^{-1} s^{-1})	
k_{t_org}	Eq. (17) (L mol^{-1} s^{-1})	[28,24]
k_{t_aq}	1×10^9 (L mol^{-1} s^{-1})	[22]
k_{act}	0.15 (L mol^{-1} s^{-1})	This work
k_{deact}	6.38×10^4 (L mol^{-1} s^{-1})	This work
k_{trm}	0.06 (L mol^{-1} s^{-1})	[26]
γ_{CuBr1}	100	This work
γ_{CuBr2}	Table 4	This work
γ_M	2030	Eq. (27) with $[M]_{aq,sat} = 3.4 \times 10^{-3}$ mol/L, Ref. [35]
k_1	2.5×10^9 (s^{-1})	Eq. (23)
k_2	1×10^8 (s^{-1})	[20]
k_3	Table 4 (s^{-1})	Eq. (23)
k_4	1×10^9 (s^{-1})	[20]
k_5	5.07×10^{10} (s^{-1})	Eq. (23)
k_6	1×10^8 (s^{-1})	[20]

Table 4
Estimated partition coefficients and transfer rate coefficient for deactivator as a function of $[CuBr_2]_0$ at 70 °C.

Range of $[CuBr_2]_0$ (mol/L)[a]	γ_{CuBr2}	k_3 (s^{-1})
$2.5 \times 10^{-3} \leq [CuBr_2]_0 < 1 \times 10^{-2}$	8.1	2.04×10^9
$1 \times 10^{-2} \leq [CuBr_2]_0 < 2.5 \times 10^{-2}$	15	3.76×10^9
$[CuBr_2]_0 > 2.5 \times 10^{-2}$	27.9	6.97×10^9

[a] Initial concentration of $CuBr_2$ relative to the organic phase volume (before mixing with the water).

4. Parameter estimation

The model requires the values of all the parameters reported in Tables 3 and 4. Most of them, such as initiator decomposition rate (k_d), average propagation rate ($\langle k_P \rangle$), termination rate (k_{t_aq}, k_{t_org}) and transfer to monomer rate (k_{trm}) constants, were taken from the literature. However, the activation rate (k_{act}), deactivation rate (k_{deact}), oligoradicals propagation rate (k_{P1}, k_{P2}) constants and partition coefficients of activator and deactivator (γ_{CuBr1}, γ_{CuBr2}) were estimated from the experimental data of Matyjaszewski et al. [7]. The estimation was performed with the commercial software gPROMS (Process Systems Enterprise, Ltd.) using the Parameter Estimation entity and the reported experimental data [7]. The constant variance model included in gPROMS was used, with a single value for all measurements. The initial values for the estimation of k_{P1}, k_{P2}, γ_{CuBr2}, and γ_{CuBr1} were selected from those reported in the literature for similar systems [20,21]. For the estimation of k_{act} and k_{deact}, we obtained the initial values from a preliminary parametric analysis.

The parameter estimation included four of the five experiments reported in Table 2, namely experiments 200/1/1, 400/1/1, 800/1/1 and 800/2/1, comprising 59 experimental measurements of $\ln\left(\frac{[M]_0}{[M]}\right)$, $\overline{M_n}$ and PDI. The remaining experiment, 400/1.5/1 (13 measurements of the same variables), and the MWD of experiment 400/1/1 (four curves at different conversions) were used for model validation.

Qiu et al. state that the partitioning of $CuBr_2$ depends on the initial $CuBr_2$ concentration ($[CuBr_2]_0$) [21]. Based on that work we proposed a stepwise functionality for the parameter γ_{CuBr2} over three ranges of $[CuBr_2]_0$ which cover those used in the experimental data reported in Table 2. A different value of γ_{CuBr2} was estimated for each concentration range.

Tables 3 and 4 report the final values of the estimated parameters as well as the parameters taken from the literature. Finally, a sensitivity analysis was performed on kinetic constants not involved in the parameter estimation, within a range of ±20% of the values reported in Table 3. The model results were insensitive to these changes.

The estimated parameters are within the orders of magnitude of the ones found in the literature for similar systems. The ATRP equilibrium constant $k_{ATRP} = k_{act}/k_{deact} = 2.4 \times 10^{-6}$ estimated in this work is near the range of reported values ($k_{ATRP} \approx 9 \times 10^{-6} - 5 \times 10^{-8}$) [36,37]. There are fewer reported values for the individual constants k_{act} and k_{deact} for systems similar to the present one. For instance, the estimated activation rate constant k_{act} is near the value of 2.05 L mol^{-1} s^{-1} reported by Tang et al. [36] for the ligand BA_6TREN and methyl methacrylate polymerization at 22 °C. The deactivation rate constant k_{deact} is lower than the value of 3.9×10^7 L mol^{-1} s^{-1} for the ligand BA_6TREN and methyl methacrylate at 22 °C, reported by the same authors. Nevertheless, the equilibrium constant k_{ATRP} is the most important value since the kinetics is mainly controlled by this equilibrium [7].

Regarding k_{P1} and k_{P2}, the values obtained are one order of magnitude larger than the average propagation rate constant $\langle k_p \rangle$. This is in agreement with the values reported in the literature for similar monomers [27].

In the case of γ_{CuBr2}, the values obtained for the three ranges are consistent with the expected behavior, that is, γ_{CuBr2} increases with $[CuBr_2]_0$. The estimated values for both γ_{CuBr2} and γ_{CuBr1} are higher than the ones reported by Qiu et al. [21] for another ligand. This was an expected result since the ligand used in this work is more hydrophobic. The transfer rate coefficient k_3 depends on the value of γ_{CuBr2}, so three values of k_3 are reported in Table 4.

It is not possible to assure that the final values of the estimated parameters are the global optimum of the estimation problem

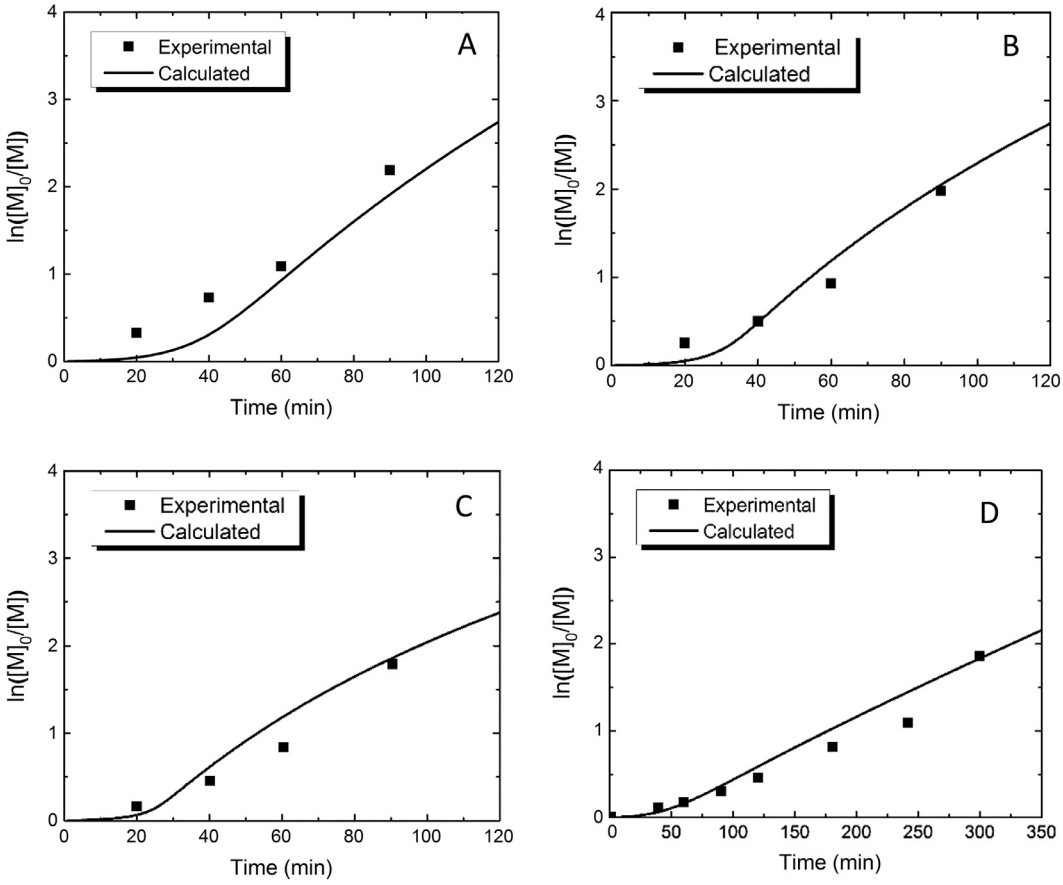

Fig. 4. Estimated and experimental first-order kinetic plots for the reverse ATRP of n-BMA in miniemulsion at 70 °C. Experiments: 200/1/1 (A), 400/1/1 (B), 800/1/1 (C), 800/2/1 (D).

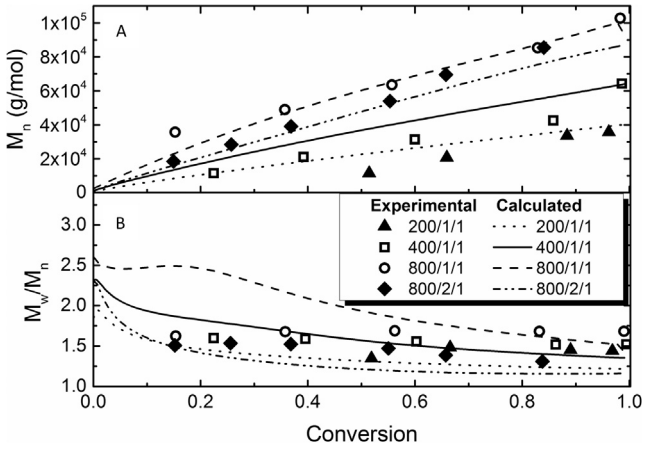

Fig. 5. Estimated and experimental number average molecular weight (A) and polydispersity (B) vs conversion for the reverse ATRP of n-BMA in miniemulsion at 70 °C.

because the process model is nonlinear and the software used does not guarantee global optimality for this case. However, the set of estimated constants allows the model to produce predictions that agree reasonably well with experimental data. As a way of evaluating the uncertainty in the parameter estimation, we have performed a sensitivity analysis on the estimated constants. Keeping all but one of the parameters constant, we evaluated the effect of changing each one by ±20%. The parameter that had the greatest effect was kp_1. For example, a change of 20% in its value resulted in an 8% change in both $\overline{M_n}$ and $\overline{M_w}$ at total conversion, with a negligible effect on the PDI.

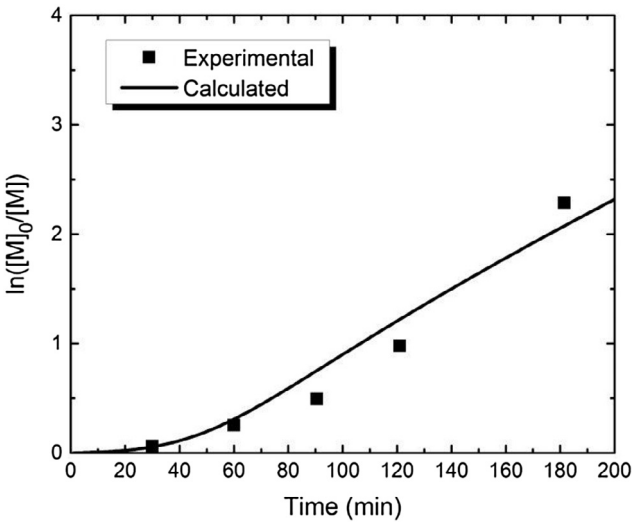

Fig. 6. Calculated and experimental first-order kinetic plot for the reverse ATRP of n-BMA in miniemulsion at 70 °C. Experiment 400/1.5/1.

5. Results and discussion

5.1. Species entry. Determination of degree of polymerization θ

The critical degree of polymerization θ was calculated for the monomer n-BMA employing Eq. (18) with $[M]_{aq,sat} = 3.4 \times 10^{-3}$ mol/L [35] and T = 343 K. This calculation yielded a value of $\theta = 2$.

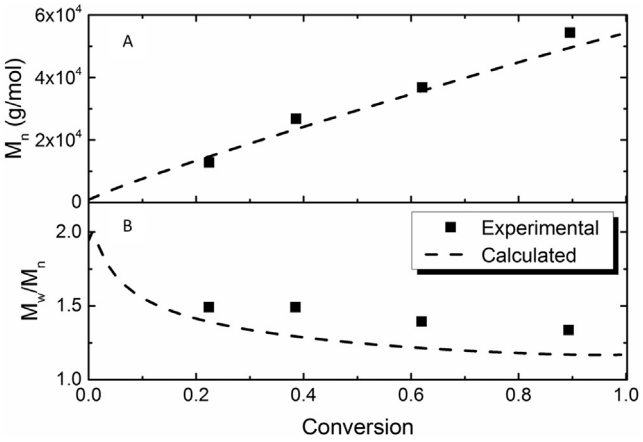

Fig. 7. Calculated and experimental number average molecular weight (A) and polydispersity (B) vs conversion for the reverse ATRP of n-BMA in miniemulsion at 70 °C. Experiment 400/1.5/1.

Maxwell et al. [22] noted that for a system where Eq. (18) gave a result of $\theta = 2$, both $\theta = 2$ and $\theta = 3$ could fit well his experimental data [22]. In order to study the influence of this parameter, we employed $\theta = 2$ as well as $\theta = 3$. Since we obtained slightly better results for the latter, $\theta = 3$ was chosen for our case study.

5.2. Prediction of experimental data

Figs. 4 and 5 compare the experimental data employed for the parameter estimation (Table 2) with the model predictions using the model parameter values reported in Tables 3 and 4.

In the case of the kinetic plots, the model predicts well the trends of the different experiments and the estimated data is in general within the range of experimental error. It can be observed that when a greater amount of $CuBr_2$ is employed, the reaction is slower, implying higher deactivation, less propagation and a better control of polymerization (Fig. 4C and D). The latter can be seen in experiment 800/2/1 where the calculated kinetic plot has a more linear dependence on time.

Additionally, the model produces a reasonable prediction of the experimental trends of $\overline{M_n}$ (Fig. 5A) and PDI (Fig. 5B) vs. conversion for the same experiments considered in Fig. 4. For example, when a higher amount of $CuBr_2$ is employed (experiment 800/2/1 versus 800/1/1), the dependence of the molecular weight with conversion becomes more linear, indicating greater control over the polymerization. This behavior is adequately followed by the model. Besides, lower molecular weights are obtained in experiment 800/2/1, since a greater number of chains are present due by the higher content of $CuBr_2$/L. A bit larger differences between experimental data and model results are observed in experiments 200/1/1 and 400/1/1. Nevertheless, as it will be shown later, the MWDs are predicted very well. The calculated coefficient of determination R^2 for all the $\overline{M_n}$ data results in a value of 0.92, indicating a good fit.

The predictions of the PDI are within the range of experimental values, with the exception of experiment 800/1/1. Here a higher polydispersity index is obtained, especially at low conversions. In fact, the model predicts a broader range of polydispersity indexes than the ones found in the experiments. It also predicts a slight decrease with conversion that is not apparent in the experimental measurements. As shown below, in spite of the differences

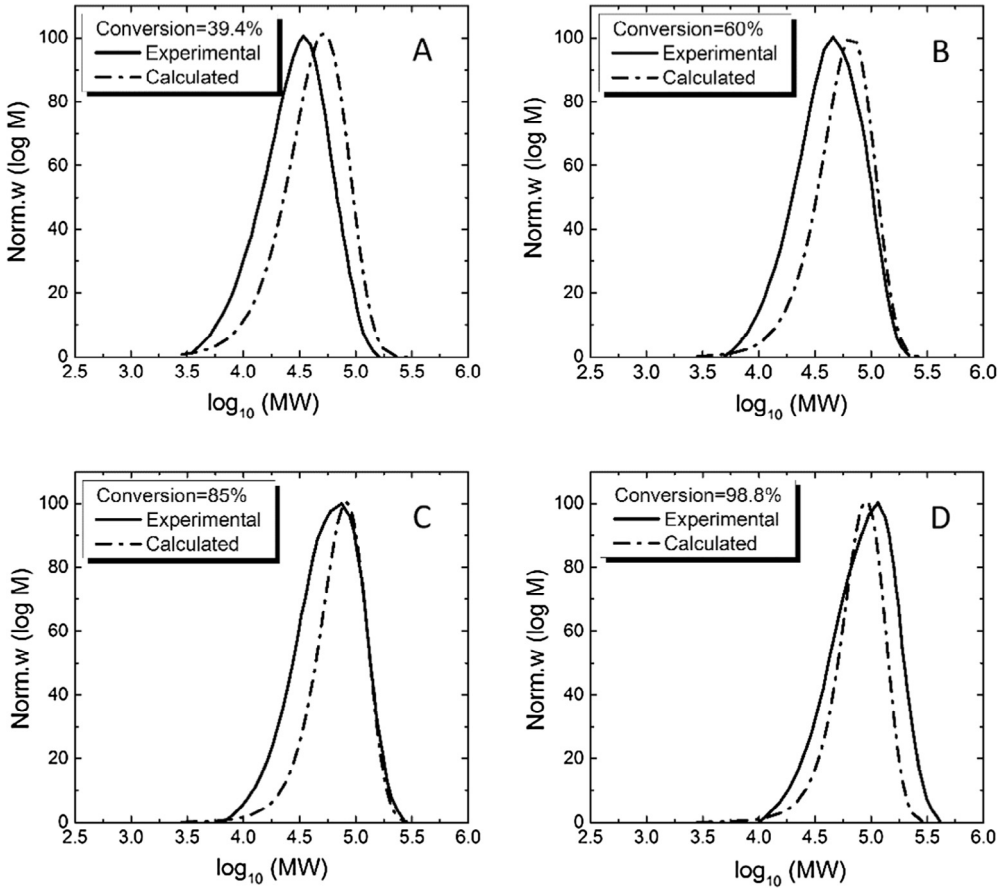

Fig. 8. Calculated and experimental molecular weight distribution at conversion of 39.4% (A), 60.0% (B), 85.0% (C) and 98.8% (D), for the reverse ATRP of n-BMA in miniemulsion at 70 °C.

obtained for the polydispersity, the predicted MWDs agree well with the experimental ones.

Experiment 400/1.5/1 was used to validate the estimation of the model parameters. It can be seen that the kinetic plot as well as the $\overline{M_n}$ and PDI profiles are predicted accurately (Figs. 6 and 7). For the latter property, the calculated values are within the range of the experimental measurements, but the same types of differences discussed for the other experiments are observed.

If we compare Figs. 4B and 6, we observe that when a higher amount of $CuBr_2$ is employed, the reaction proceeds more slowly, implying higher deactivation and a better control of polymerization reaction. The latter is evidenced in the more linear dependence of the kinetic plot shown in Fig. 6.

Finally, the predicted and experimental MWDs for experiment 400/1/1 at four different conversions are shown in Fig. 8. The agreement between simulated and experimental MWDs is good. As conversion increases, the MWDs shift towards higher molecular weights. The observed differences correspond to the deviations previously discussed, but the shape and the location of the distributions agree well with the experimental data.

6. Conclusions

In this work, we propose a mathematical model for a reverse ATRP in miniemulsion using a water-soluble initiator. The model is based on the mass balance equations of the reacting species. The reactions in both the aqueous and organic phases, as well as the mass transfer between them, were considered. The model allows predicting average molecular properties, such as number and weight average molecular weights, as well as the full molecular weight distribution (MWD) for different experimental conditions where particles are larger than 200 nm. The average properties were calculated using the method of moments and the MWD was obtained by means of the pgf technique. The combination of both mathematical techniques was successful in describing the process behavior.

Simulations took a very short time on a standard desktop computer, making the model a suitable tool to be included in an optimization framework. Some of the constants required by the model were estimated, employing literature experimental data. The model performance was evaluated with other sets of literature experimental data, showing good quality predictions. This result also shows that the pgf technique can be successfully applied to dispersed systems, showcasing the versatility of this mathematical technique.

Overall, this work presents a valuable tool able to predict the main molecular properties of the product synthesized by a reverse ATRP in miniemulsion using a water-soluble initiator. The model presented in this work may be included in an optimization frame to allow predicting operating conditions for obtaining a prespecified polymer product. Work is under way to extend the model for systems with smaller particles.

Acknowledgments

The authors thank the financial support of CONICET (Consejo Nacional de Investigaciones Científicas y Técnicas, Argentina) and UNS (Universidad Nacional del Sur, Argentina).

References

[1] M.F. Cunningham, Controlled/living radical polymerization in aqueous dispersed systems, Prog. Polym. Sci. 33 (4) (2008) 365–398.
[2] J.K. Oh, Recent advances in controlled/living radical polymerization in emulsion and dispersion, J. Polym. Sci. Part Polym. Chem. 46 (21) (2008) 6983–7001.
[3] P.B. Zetterlund, Y. Kagawa, M. Okubo, Controlled/living radical polymerization in dispersed systems, Chem. Rev. 108 (9) (2008) 3747–3794.
[4] J. Qiu, B. Charleux, K. Matyjaszewski, Controlled/living radical polymerization in aqueous media: homogeneous and heterogeneous systems, Prog. Polym. Sci. 26 (10) (2001) 2083–2134.
[5] K. Matyjaszewski, T.P. Davis (Eds.), Handbook of Radical Polymerization, Wiley-Interscience, Hoboken, 2002.
[6] K. Matyjaszewski, Atom transfer radical polymerization (ATRP): current status and future perspectives, Macromolecules 45 (10) (2012) 4015–4039.
[7] M. Li, K. Matyjaszewski, Reverse atom transfer radical polymerization in miniemulsion, Macromolecules 36 (16) (2003) 6028–6035.
[8] R.W. Simms, M.F. Cunningham, Reverse atom transfer radical polymerization of butyl methacrylate in a miniemulsion stabilized with a cationic surfactant, J. Polym. Sci. Part Polym. Chem. 44 (5) (2006) 1628–1634.
[9] R.W. Simms, M.F. Cunningham, High molecular weight poly(butyl methacrylate) by reverse atom transfer radical polymerization in miniemulsion initiated by a redox system, Macromolecules 40 (4) (2007) 860–866.
[10] M. Li, K. Min, K. Matyjaszewski, ATRP in waterborne miniemulsion via a simultaneous reverse and normal initiation process, Macromolecules 37 (6) (2004) 2106–2112.
[11] Y. Kagawa, P.B. Zetterlund, H. Minami, M. Okubo, Atom transfer radical polymerization in miniemulsion: partitioning effects of Copper(I) and Copper (II) on polymerization rate, livingness, and molecular weight distribution, Macromolecules 40 (9) (2007) 3062–3069.
[12] P.B. Zetterlund, Compartmentalization effects on bimolecular termination in atom transfer radical polymerization in nanoreactors: compartmentalization effects on bimolecular termination in atom transfer radical, Macromol. Theory Simul. 20 (8) (2011) 660–666.
[13] Y. Kagawa, P.B. Zetterlund, H. Minami, M. Okubo, Compartmentalization in atom transfer radical polymerization (ATRP) in dispersed systems, Macromol. Theory Simul. 15 (8) (2006) 608–613.
[14] P.B. Zetterlund, Y. Kagawa, M. Okubo, Compartmentalization in atom transfer radical polymerization of styrene in dispersed systems: effects of target molecular weight and halide end group †, Macromolecules 42 (7) (2009) 2488–2496.
[15] P.B. Zetterlund, Compartmentalization in atom transfer radical polymerization to high conversion in dispersed systems: effects of diffusion-controlled reactions, Macromolecules 43 (3) (2010) 1387–1395.
[16] M.E. Thomson, M.F. Cunningham, Compartmentalization effects on the rate of polymerization and the degree of control in ATRP aqueous dispersed phase polymerization, Macromolecules 43 (6) (2010) 2772–2779.
[17] H. Tobita, Kinetics of controlled/living radical polymerization in emulsified systems, Macromol. Symp. 261 (1) (2008) 36–45.
[18] H. Tobita, Modeling controlled/living radical polymerization kinetics: bulk and miniemulsion, Macromol. React Eng. 4 (11–12) (2010) 643–662.
[19] H. Tobita, Effects of fluctuation and segregation in the rate acceleration of ATRP miniemulsion polymerization, Macromol Theory Simul. 20 (3) (2011) 179–190.
[20] J.W. Ma, M.F. Cunningham, K.B. McAuley, B. Keoshkerian, M. Georges, Nitroxide mediated living radical polymerization of styrene in miniemulsion—modelling persulfate-initiated systems, Chem. Eng. Sci. 58 (7) (2003) 1177–1190.
[21] J. Qiu, T. Pintauer, S.G. Gaynor, K. Matyjaszewski, B. Charleux, J.-P. Vairon, Mechanistic aspect of reverse atom transfer radical polymerization of *n*-butyl methacrylate in aqueous dispersed system, Macromolecules 33 (20) (2000) 7310–7320.
[22] I.A. Maxwell, B.R. Morrison, D.H. Napper, R.G. Gilbert, Entry of free radicals into latex particles in emulsion polymerization, Macromolecules 24 (7) (1991) 1629–1640.
[23] K.A. Payne, D.R. Dhooge, P.H.M. Van Steenberge, et al., ARGET ATRP of butyl methacrylate: utilizing kinetic modeling to understand experimental trends, Macromolecules 46 (10) (2013) 3828–3840.
[24] W. Wang, R.A. Hutchinson, M.C. Grady, Study of butyl methacrylate depropagation behavior using batch experiments in combination with modeling, Ind. Eng. Chem. Res. 48 (10) (2009) 4810–4816.
[25] M.N. Siddiqui, H.H. Redhwi, G.D. Verros, D.S. Achilias, Evaluating the role of nanomontmorillonite in bulk in situ radical polymerization kinetics of butyl methacrylate through a simulation model, Ind. Eng. Chem. Res. 53 (28) (2014) 11303–11311.
[26] D.F. Sangster, J. Feldthusen, J. Strauch, C.M. Fellows, Measurement of transfer coefficients to monomer for *n*-butyl methacrylate by molecular weight distributions from emulsion polymerization, Macromol. Chem. Phys. 209 (15) (2008) 1612–1627.
[27] S. Beuermann, M. Buback, Rate coefficients of free-radical polymerization deduced from pulsed laser experiments, Prog. Polym. Sci. 27 (2) (2002) 191–254.
[28] M. Buback, T. Junkers, Termination kinetics of tert-butyl methacrylate and of n-butyl methacrylate free-radical bulk homopolymerizations, Macromol. Chem. Phys. 207 (18) (2006) 1640–1650.
[29] M. Asteasuain, C. Sarmoria, A. Brandolin, Recovery of molecular weight distributions from transformed domains. Part I. Application of pgf to mass balances describing reactions involving free radicals, Polymer 43 (8) (2002) 2513–2527.
[30] A. Brandolin, A. Assini Balbueno, M. Asteasuain, Improved numerical inversion methods for the recovery of bivariate distributions of polymer properties from

2D probability generating function domains, Comput. Chem. Eng. 94 (2016) 272–286.
[31] A. Brandolin, C. Sarmoria, A. López-Rodríguez, K.S. Whiteley, B. Del Amo Fernandez, Prediction of molecular weight distributions by probability generating functions. Application to industrial autoclave reactors for high pressure polymerization of ethylene and ethylene-vinyl acetate, Polym. Eng. Sci. 41 (2001) 1413–1426.
[32] C. Fortunatti, C. Sarmoria, A. Brandolin, M. Asteasuain, Modeling of the bivariate molecular weight distribution-copolymer composition distribution in RAFT copolymerization using probability generating functions, Comput. Mater. Sci. 136 (2017) 280–296.
[33] C. Fortunatti, C. Sarmoria, A. Brandolin, M. Asteasuain, Modeling of RAFT polymerization using probability generating functions. Detailed prediction of full molecular weight distributions and sensitivity analysis, Macromol. React. Eng. 8 (2014) 781–795.
[34] S. Beuermann, M. Buback, T.P. Davis, Critically evaluated rate coefficients for free-radical polymerization, 3a. Propagation rate coefficients for alkyl methacrylates, Macromolcular Chem. Phys. 201 (12) (2000) 1355–1364.
[35] R. de Vries, C.C. Co, E.W. Kaler, Microemulsion polymerization. 2. Influence of monomer partitioning, termination, and diffusion limitations on polymerization kinetics, Macromolecules 34 (10) (2001) 3233–3244.
[36] W. Tang, Y. Kwak, W. Braunecker, N.V. Tsarevsky, M.L. Coote, K. Matyjaszewski, Understanding atom transfer radical polymerization: effect of ligand and initiator structures on the equilibrium constants, J. Am. Chem. Soc. 130 (32) (2008) 10702–10713.
[37] W. Tang, N.V. Tsarevsky, K. Matyjaszewski, Determination of equilibrium constants for atom transfer radical polymerization, J. Am. Chem. Soc. 128 (5) (2006) 1598–1604.